HHS Public Access

Author manuscript

Soft Matter. Author manuscript; available in PMC 2019 November 25.

Published in final edited form as:

Soft Matter. 2019 February 06; 15(6): 1269–1277. doi:10.1039/c8sm02059k.

The stabilization of primitive bicontinuous cubic phases with tunable swelling over a wide composition range†

Sherry S. W. Leung, **Cecilia Leal**

Department of Materials Science and Engineering, University of Illinois at Urbana, Champaign, USA.

Abstract

In this paper we investigate the pseudo-ternary phase diagram of glycerol monooleate (GMO), a cationic lipid (DOTAP - 1,2-dioleoyl-3-trimethylammonium propane), and a ″PEGylated″ lipid (DOPE-PEG - 1,2-dioleoyl-*sn-glycero*-3-phosphoethanolamine-*N*-[methoxy(polyethylene glycol)-2000 kDa]) in excess water. We use small angle X-ray scattering (SAXS) and cryogenic transmission electron microscopy (Cryo-EM) to map out a phase diagram in a regime of low DOPE-PEG content (1–5 mol%), which is pertinent for the application of lipid systems as carriers of biomolecular cargo to cells. Pure GMO is known to self-assemble into bicontinuous cubic phases of the gyroid type at low water content and of the diamond type in excess water. These complex structures have numerous advantages reaching beyond drug delivery, *e.g.* as protein crystallization matrices, but their formulation is challenging as very small contents of guest molecules can shift the phase behavior towards other geometries such as the lamellar phase. In this work, we show that the ternary GMO/DOTAP/DOPE-PEG system allows the stabilization of bicontinuous cubic phases in excess water over a wide composition range. The symmetry of the phase can be tuned by varying the amount of PEGylated lipid, with the primitive type dominating at low DOPE-PEG content (1–3 mol%) and the diamond phase arising at 5 mol% DOPE-PEG. In addition, we found that the diamond phase is virtually non-responsive to electrostatic swelling. In contrast, primitive bicontinuous cubic lattice dimensions swell up in equilibrium to 650 A with increased cationic lipid content.

Introduction

Lipid bicontinuous phases are found in biological systems[1,2] and have numerous biotechnology applications, including drug delivery,[3,4] nucleic acid delivery,[5–8] biosensing,[9,10] medical imaging,[4,11,12] membrane protein crystallization,[13–16] and foods.[17] Fig. 1 illustrates the structures of bicontinuous cubic phases that are commonly found with certain lipid systems. These structures can be categorized by their crystallographic space group symmetries: the gyroid cubic $\left(Q_{II}^{G} \text{ or } Ia3d\right)$, the primitive cubic $\left(Q_{II}^{P} \text{ or } Im3m\right)$, or the diamond

†Electronic supplementary information (ESI) available. See DOI: 10.1039/c8sm02059k

cecilial@illinois.edu.

Conflicts of interest

There are no conflicts to declare.

cubic $\left(Q_{II}^{D} \text{ or } Pn3m\right)$. These highly ordered structures consist of a continuously folded lipid bilayer that separates two independent water channel networks.[18,19] The formation of these structures is entropically favorable[20] and satisfies lipid molecular packing of certain lipids, most notably monoolein (also known as glycerol monooleate or GMO) and phythantriol.[21,22] The application of bicontinuous cubic phases for the encapsulation of small molecules, nucleic acids, and proteins has propelled efforts to control the size of the unit cell and concomitantly, the diameter of the water channels.[13,23–29] With GMO and water, one can obtain two types of cubic phases at low (gyroid cubic) and high (diamond cubic) water content.[30] Recently we have shown that a lipid mixture of GMO, DOTAP (1,2-dioleoyl-3-trimethylammonium propane), and GMO-PEG (custom designed GMO covalently linked to polyethylene glycol 2 kDa) in excess water enables the stabilization of highly ordered bicontinuous cubic phases in excess water of all three symmetry groups (gyroid, diamond, and primitive), with tunable lattice dimensions (a^{Q} = 150–680 Å).[6,25] The resultant cubic phase retains order, as in a single-crystal, and lattice dimension for an extended period of time (> 6 months). Tuning of both symmetry group and lattice size can be achieved by varying composition as well as processing conditions.

The lattice spacing of bicontinuous cubic phases in equilibrium with water is directly related to the diameter of the water channels. However, due to the topological parameters of the different space groups, primitive lattices have wider channels than gyroid and diamond phases, for the same lattice size.[31,32] As a result, primitive lattices are generally preferred for hosting molecular species and are more likely to retain their structure upon encapsulation. One specific example is the GMO/DOTAP/GMO-PEG lipid system where the primitive phase persists after incorporation of short length RNA molecules (siRNA), whereas incorporation of siRNA into the gyroid cubic phase of GMO/DOTAP/GMO-PEG led to a transformation to a hexagonal phase.[6] The robustness of the primitive bicontinuous cubic phase upon siRNA encapsulation may also be due to differences in membrane elasticity. Another example is the incorporation of as little as 0.1 wt% insulin has been shown to disrupt the gyroid structure of GMO.[33] Polymeric primitive structures have been shown to have a relative elastic modulus twice that of the diamond or the gyroid phase.[34] Finding a lipid system with structural stability of the primitive bicontinuous cubic phase over a wide composition space will benefit numerous applications including the development of robust matrices to guide protein crystallization as well as the delivery of cargo to cells.

In this paper, we employ small angle X-ray scattering (SAXS) and cryogenic transmission electron microscopy (Cryo-EM) to explore the ternary lipid mixture of GMO, DOTAP, and negatively charged 1,2-dioleoyl-*sn-giycero*-3-phosphoethanolamine-*N*-[methoxy(polyethylene glycol)-2000 kDa] (DOPE-PEG) in excess water in a compositional regime relevant for the design of siRNA[6,8] and drug[35] delivery systems. All three lipids are commercially available, in contrast to the analogous ternary lipid mixture used in our previous studies[6,8,25] where custom synthetized neutral GMO-PEG was used as the PEGylated lipid. Fig. 2 shows the structures of the three lipids used in this work. We found that the space group symmetry of the preferred cubic structure formed is strongly dependent on the type of PEGylated lipid used and their concentration. Our findings suggest that the chosen lipid mixture forms bicontinuous cubic phases with preferred properties for

applications in siRNA delivery as well as protein crystallization because (i) the primitive cubic phase dominates a relatively large part of the phase diagram, and (ii) this mixture is capable of forming cubic phases with extremely large water channels. Earlier work showed that guest molecules can induce a transition from the cubic phase to the hexagonal phase.[36,37] Kim *et al.* showed that only the primitive cubic phase was resistant to phase changes upon incorporation of siRNA.[6] Kim *et al.* also showed that larger water channels with lower curvature are more favorable for inclusion of guest molecules that are rather stiff such as gold nanoparticles.[25] This work has direct relevance for designing both bulk and lipid nanoparticle delivery systems and contributes to the understanding of swollen lipid bicontinuous cubic phases.

Results

The influence of negatively charged DOPE-PEG inclusion on a GMO/DOTAP binary system as probed by SAXS

We systematically explored part of the GMO/DOTAP/DOPE-PEG phase diagram at the low PEGylated lipid content regime, which is relevant for the applications of siRNA and drug delivery to cells. Fig. 3 shows representative radially integrated SAXS diffractograms for the ternary lipid mixture GMO/DOTAP/DOPE-PEG at varied compositions in excess water. The ratios of q values for the diffraction peaks are used to determine the Miller indices for each peak and reveal the identity of the phases present.[38] Fig. 3A shows SAXS data obtained for the GMO/DOTAP/DOPE-PEG system at fixed DOPE-PEG concentration (1 mol%). The existence of a lamellar phase is revealed at low GMO content (20: 79: 1, molar percentages). The characteristic equally spaced Bragg reflections arising from the [100], [200], [300], [400], and [500] planes can be observed and the lamellar repeat spacing is $d = 2\pi/q_{[100]} =$ 279 Å. In a regime of intermediate GMO content (50: 49 : 1), Bragg reflections arising from a lamellar phase ($d = 330$ Å) are observed in coexistence with peaks at the relative ratios $\sqrt{2}, \sqrt{3}, \sqrt{4}, \sqrt{6}, \sqrt{8},$ *etc.*, characteristic of a diamond cubic phase. The absolute q position of the peaks corresponds to a lattice spacing $a\left(\mathrm{Q}_{\mathrm{II}}^{\mathrm{D}}\right)$ of 522 Å. At high GMO content (91 : 8 :1), the Bragg peaks follow the ratios of $\sqrt{2}, \sqrt{4}, \sqrt{6}, \sqrt{10}, \sqrt{12},$ *etc.*, which are indexed to a bicontinuous cubic phase of the primitive type with a lattice spacing $a\left(\mathrm{Q}_{\mathrm{II}}^{\mathrm{P}}\right)$ of 444 Å. All these systems are equilibrated in excess water and it is clear that variations in GMO content enable a rather rich phase space. Fig. 3B shows the SAXS data for a GMO/DOTAP/DOPE-PEG system where the percentage of DOPE-PEG is increased to 5 mol% (86: 9: 5) and the Bragg peaks are consistent with a bicontinuous cubic phase of the diamond type with a lattice spacing $a\left(\mathrm{Q}_{\mathrm{II}}^{\mathrm{G}}\right)$ of 293 Å. Analogous to what was observed when custom synthetized GMO-PEG was added to the GMO/DOTAP system,[6] the ratio of GMO/DOTAP and the content of PEGylated lipid modulates the identity of the bicontinuous cubic phase. However, we found that DOPE-PEG permits the persistence of bicontinuous primitive cubic phase for a wider composition range. In the GMO/DOTAP binary mixtures without DOPE-PEG, the gyroid cubic phase exist between 85–100 mol% GMO.[5] Similarly, bicontinuous cubic phases were observed in GMO/DOTAP/DOPE-PEG in the presence of *ca.* 85–100 mol% GMO. We found that at high GMO content (>85:15 GMO/DOTAP) the concentration of DOPE-PEG can be changed from at least 1–3 mol% without affecting the symmetry group

of the equilibrium bicontinuous cubic phase observed. This is in contrast to what was observed for the GMO/DOTAP system using GMO-PEG, where the addition of only 1 mol % switched a primitive lattice to a gyroid one.[6] Fig. 3C shows a GMO/DOTAP (92 : 8, molar percentage) mixture with added DOPE-PEG. Addition of 1–3 mol% DOPE-PEG retains a bicontinuous primitive cubic phase with lattice dimensions of 290–472 Å. At 5 mol % DOPE-PEG the system switches to the diamond symmetry group. Clearly, small amounts of PEGylated lipids have the ability to alter the unit cell dimensions as well as crystallographic group. This behavior is observed for different types of PEGylated lipid. Even though all G, P, and D phases are topologically identical, there are important differences with respect to membrane elasticity and molecular packing that make one group favorable over the other depending on the molecular system.[22] Note that the 1 and 2 mol% DOPE-PEG samples were hydrated with a different amount of water than the 3 and 5 mol% DOPE-PEG samples (see Materials and Methods). Table S1 in the ESI† summarizes all phases and lattice dimensions information from SAXS experiments. SAXS data presented are collected at room temperature or 22 °C. Data collected at 36 °C (Fig. S1, ESI†) shows that the observed cubic phases are likely stable at physiological temperatures as well.

The structure of GMO/DOTAP/DOPE-PEG ternary lipid mixtures as probed by Cryo-EM

Fig. 4 shows that the SAXS structural observations of GMO/DOTAP/DOPE-PEG mixtures (shown in Fig. 3) are corroborated by Cryo-EM. Each point on the phase diagram represents a unique composition of the GMO/DOTAP/DOPE-PEG mixture. This enlarged region of the pseudo-ternary phase diagram highlights the area most relevant for development of siRNA-lipid delivery systems, *i.e.,* at low DOPE-PEG concentrations (1–5 mol%). For all DOPE-PEG concentrations studied, the lamellar phase dominates the low GMO regime (0: 100 to 50: 50 GMO/DOTAP). In the high GMO regime (50: 50 to 100: 0 GMO/DOTAP), there are two types of cubic phases observed in GMO/DOTAP/DOPE-PEG mixtures: primitive (low DOPE-PEG content) and diamond (higher DOPE-PEG content). Equilibration in complex lipid mixtures such as those presented here can be sluggish: the symmetry group, as well as the lattice spacing of bicontinuous cubic phases, can be trapped in metastable states.[25] In this work, samples were equilibrated for a very long time and inspected multiple times before the construction of the phase diagram. However, certain samples display unexpected coexistence of, as well as re-entrant, lamellar phases at high GMO content. At some intermediate compositions (see $X_{GMO} = 50$ in Fig. 3A), phase coexistence is observed as a superposition of two sets of SAXS diffraction patterns. In fact, the SAXS diffraction patterns can be rather difficult to interpret at GMO/DOTAP molar percentages between 50: 50 and 80 : 20 for all DOPE-PEG concentrations and Cryo-EM was used to assist with the structure determination. For this technique samples are embedded in a thin layer of vitreous ice that preserves the native, hydrated state of the lipid structure.[39,40] The Cryo-EM images at high and low GMO content are consistent with the SAXS data: multilamellar structures are visible at low GMO concentrations, and bicontinuous cubic phases of the space group identified from SAXS were seen at high GMO content. For example, concentric circles with even spacing between the bilayers in 30:70: 1 GMO/DOTAP/DOPE-PEG correspond to multilamellar vesicles. The distance between the bilayers measures *ca.* 20 nm, consistent with lamellar repeat spacing measured using SAXS. At GMO contents above 50 mol%, bicontinuous cubic phases are found for DOPE-PEG contents varying from 1–5 mol%. In

certain orientations, bicontinuous cubic phases can appear as a rectangular grid, as is observed for the 59 : 40 : 1 and 91 : 6: 3 GMO/DOTAP/DOPE-PEG samples, both being of the primitive type. The absence of the {111} reflection in the fast Fourier transforms (FFT) of these micrographs identifies the space group as primitive cubic (see insets of Cryo-EM images).[41] The coexistence of rectangular grid (not shown) and hexagonal features in the FFT of 76 : 19 : 5 GMO/DOTAP/DOPE-PEG verifies the presence of the diamond cubic phase.[41]

Cryo-EM imaging takes place under vacuum and some image artifacts arise due to some degree of freeze-drying.[42] Image analysis reveal a lattice dimension $a\left(Q_{II}^{D}\right)$ of 330 Å for GMO/DOTAP/DOPE-PEG 59 : 40 : 1 and $a\left(Q_{II}^{D}\right) = 180\text{Å}$ for 91 : 6: 3. These values are smaller than those measured with SAXS and are consistent with some level of dehydration. Thus, the extraction of lattice dimensions is more reliable using SAXS, which is a technique that interferes the least with the sample native state. It is noteworthy that bicontinuous cubic phases, which are relatively rigid and have high storage moduli,[4,43,44] seem to withstand the freeze-drying processes - a common method for improving the long term stability of colloidal systems.[45–48]

Discussion

DOPE-PEG enables the stabilization of bicontinuous phases over a wide composition range

Loading guest molecules into the cubic phase can lead to modified structural parameters, or undesirable phase changes.[25,33,37,49–53] First, we treat the PEGylated lipids as a guest molecule of the binary GMO/DOTAP lipid matrix. Previously, our group showed that the cubic structures of GMO/DOTAP can accommodate GMO-PEG, a custom synthesized PEGylated GMO.[6] The use of DOPE-PEG in this paper adds an entire 18 carbon chain onto the PEGylated lipid. In both ternary lipid mixtures, all three lipids have the same 18 carbon chains, namely one with a double bond between carbon 9 and 10. It is surprising that moderate amounts of DOTAP and bulky DOPE-PEG is tolerated in the cubic phase, and that 20 mol% DOTAP along with at least 5 mol% DOPE-PEG can be incorporated without inducing a transition to the lamellar phase. In comparison, GMO cubic phases in binary systems can accommodate a moderate amount of DOPC (20 mol%), DOPE (20 mol%), and cholesterol (20 mol%), and a smaller amount of DOPS (7 mol%), diacylglycerol and triacylglycerol (5 mol%), fatty acids (10 mol%), lyso-PC (10 mol%), cardiolipin (6 mol%), DMPE-mPEG550 (3 mol%), gadolinium(III)-diethylenetriaminepentaacetic acid-GMO (5 mol% in bulk and 1 mol% in dispersions).[11,14,54,55] We hypothesize that the addition of bulky DOPE-PEG does not prevent the formation of bicontinuous cubic structure because DOPE-PEG is negatively charged and can bind electrostatically with the positively charged head group of DOTAP, forming the required molecular packing for bicontinuous cubic phase formation. This may explain why, in the presence of DOPE-PEG, up to 20 mol% charged lipid DOTAP is tolerated in the cubic structure when only up to 7 mol% charged lipid DOPS can be incorporated into GMO/DOPS cubic structures.[14]

In our previous work, small changes in GMO-PEG content led to dramatic changes in phase behavior.[6] For example, 95 : 4: 1 GMO/DOTAP/GMO-PEG forms a well-ordered primitive cubic phase and 95 : 3 : 2 GMO/DOTAP/GMO-PEG forms the gyroid phase with a very different lattice spacing $\left[a\left(\mathrm{Q}_{\mathrm{II}}^{\mathrm{P}}\right)=160\text{Å}\ vs.\ a\left(\mathrm{Q}_{\mathrm{II}}^{\mathrm{G}}\right)=217\ \text{Å}\right]$. At 95 : 2 : 3 GMO/DOTAP/GMO-PEG, the gyroid phase coexists with the lamellar phase. These results suggest that these compositions are close to a phase boundary. Since these compositions are close to the exterior edge of the phase diagram, they also suggest that the primitive phase occupies an extremely small region of the phase diagram. This is illustrated in the partial phase diagram for GMO/DOTAP/GMO-PEG constructed with data from Kim *et al.*[6] in Fig. 5, and its relevance is discussed in the next section. A small change in the lipid ratio could cause a transformation to a different phase, and incorporation of a guest molecule is also likely to induce a phase change. The use of DOPE-PEG instead of GMO-PEG is advantageous because it is commercially available. Importantly, the phase behavior of the GMO/DOTAP/PEGylated lipid is considerably richer with all three phases (primitive, gyroid, and diamond) in a significantly wide composition range. Importantly, we expect GMO-PEG and DOPE-PEG to be fully incorporated within the bicontinuous cubic structures. Even though both lipids have the ability to form micelles, PEGylated lipids are known to preferentially locate within lipid bilayers up to a nominal composition of at least 8 mol%.[56]

If we now consider siRNA, a drug, or a protein as the guest molecule in the bicontinuous cubic phase of GMO/DOTAP/PEGylated lipid, one can expect that depending on size and physicochemical properties (*e.g.* charge), restructuring may occur as well. The incorporation of long negatively charged nucleic acids is known to promote transitions from bicontinuous cubic to hexagonal phases for example.[37] This is consistent with the previous observation that the incorporation of siRNA into the gyroid cubic phase of GMO/DOTAP/GMO-PEG led to a transformation to the hexagonal phase.[6] Interestingly, the same system at a composition where the primitive phase was present remained stable even after siRNA inclusion. It is therefore beneficial that the primitive structure is the dominant bicontinuous cubic structure when DOPE-PEG is used; in contrast the gyroid was more prominent in the GMO-PEG system (see Fig. 5). Moreover, the primitive cubic phase region of the GMO/DOTAP/DOPE-PEG system is larger than other PEGylated GMO mixtures in the literature: up to 20 mol% DOTAP can be used to form a pure primitive cubic phase. For example, in mixtures of GMO, egg yolk phosphatidylcholine (eggPC), and 8 wt% Pluronic F127 (triblock polymer PEO99-PPO67-PEO99, where PEO and PPO denote hydrophilic poly-(ethylene oxide) and lipophilic poly(propylene oxide), respectively[57]), the following phase progression was observed: GMO/eggPC ratio of 0 : 100 to 50 : 50 is lamellar, 60 : 40 to 65 : 45 is likely coexistence of lamellar and cubic, 70 : 30 is primitive, 80 : 20 is coexistence of primitive and diamond, and 90: 10 to 100: 0 is diamond cubic.[58] Similarly, in ternary mixtures of GMO/cationic amphiphile dioctadecyldimethylammonium bromide (DOMA)/DOPE-PEG2000 in excess buffer (NaH_2PO_4/Na_2HPO_4, 1×10^{-2} M, pH 7, 1 wt% lipid),[59,60] diamond and primitive coexists in 82 : 15 : 3 GMO/DOMA/DOPE-PEG2000. Another example can be found in mixtures involving *cis*-5,8,11,14,17-eicosapentaenoic acid (20: 5 ω −3 polyunsaturated fatty acid, EPA): 90 : 10 GMO/EPA + 2 mol% DOPE-PEG2000 is cubic, but mixtures with higher EPA content (80: 20 to 50:50 GMO/EPA) formed mixtures of non-lamellar and lamellar structures.[61]

The larger unit cells of GMO/DOTAP/DOPE-PEG bicontinuous cubic structures

Tuning water channel size is important for encapsulation and release of the active ingredient, as well as in the use of bicontinuous cubic phases to guide the crystallization of proteins.[13] SAXS data provides lattice dimensions in addition to unambiguous space group symmetry assignment. Fig. 6A shows a plot of the wave-vector, q, peak positions *versus* $(h^2 + k^2 + l^2)^{1/2}$, where *h, k, l* are the Miller indices assigned to each peak based on the assumption of primitive cubic symmetry. The linear relationship between these two quantities confirms the primitive cubic assignment for both 95 : 4 : 1 GMO/DOTAP/DOPE-PEG and 95 : 4: 1 GMO/DOTAP/GMO-PEG. The slope of the line is equal to $2\pi/a^{Q}$, where a^{Q} is the lattice dimension of the cubic phase. For the primitive cubic phase formed in 95 : 4 : 1 GMO/DOTAP/DOPE-PEG, the lattice spacing $a\left(Q_{II}^{P}\right)$ is 484 Å. For comparison, replacing DOPE-PEG with GMO-PEG results in $a\left(Q_{II}^{P}\right) = 160$ Å.[6] These correspond to estimated water channel diameters (d_W) (eqn (3)) of 276 Å and 65 Å, respectively. The size of the water channels in the DOPE-PEG system are more than quadruple those in the GMO-PEG system. Larger water channels should be more favorable for inclusion of rigid, rod-like siRNA molecules and for incorporating other larger and more molecules.[29,36,62,63] It is important to note that these values are obtained for a system in thermodynamic equilibrium. We have shown before that bicontinuous cubic phases can be processed out of equilibrium:[25] *i.e.,* we synthesized kinetically trapped single-crystals with lattice dimensions (a^{Q}) of 680 Å. However, this fact is unrelated to temporal stability and these materials retain their crystallinity and lattice dimension for over 6 months. The samples prepared in this work however were processed such that thermodynamic equilibrium is likely attained.

Calculations by Bruinsma *et al.* suggested an upper limit on cubic phase lattice parameters of *ca.* 300 Å,[23] but larger lattice parameters have been repeatedly reported recently.[13,24–26,59] Barriga *et al.* demonstrated that primitive phases with lattice parameter of 480 Å exist in 65 : 5 : 30 GMO/DOPS/cholesterol at 54 °C.[24] In comparison, the ternary lipid mixture presented in this paper GMO/DOTAP/DOPE-PEG achieves this level of swelling at room temperature (at 22 °C). Near room temperature (at 26 °C), the lattice parameter of GMO/DOPS/cholesterol drops to *ca.* 440 Å.[24] Angelov *et al.* studied ternary mixtures of GMO, dioctadecyldimethylammonium bromide (DOMA), and DOPE-PEG dispersed in excess aqueous phosphate buffer medium, and found coexistence of primitive and diamond nanoparticles with lattice spacings of 351 Å and 280 Å, respectively, in 82 : 15 : 3 GMO/DOMA/DOPE-PEG mixtures.[59,60] The components of this mixture are similar to GMO/DOTAP/DOPE-PEG used in this work, and suggests that the presence of the cationic species[5,14,25,26,29,54,59,64] and PEGylated lipids[6,59] are responsible for the swelling observed in both of these ternary lipid mixtures. As shown in Fig. 6B and Fig. S2 (ESI†), the lattice parameter of GMO/DOTAP/DOPE-PEG primitive cubic structure increases in a dose dependent manner on cationic lipid content of the ternary mixture as opposed to the diamond lattice (at 5 mol% DOPE-PEG) that remains essentially unchanged. Fig. S3 (ESI†) shows that this trend is conserved regardless of the initial lattice spacing value which can be different depending on water content. This is consistent with primitive lattices being

elastically more robust,[34] as it has been postulated that thermal fluctuations of the lipid bilayers within bicontinuous cubic phases are the limiting factor to lattice swelling above 300 Å.[23] In light of the earlier discussion on electrostatic swelling, it is surprising that the diamond cubic phase lattice repeat spacing remained constant with increasing cationic lipid content when 5 mol% DOPE-PEG is present. There is some evidence of electrostatic shrinking in diamond phases in the literature, however. Nazaruk *et al.* observed shrinkage of the diamond cubic lattice spacing when cationic additive *N*-(2-aminoethyl)oleamide was added to GMO.[65] Shrinkage of the diamond cubic lattice has also been observed in binary mixtures of GMO and lipid-like anionic peptides with high peptide concentrations prior to a diamond to hexagonal phase transition.[66]

Water channel size is known to alter diffusion, transport properties, and drug release profile, our findings thus provide an additional handle on controlling payload release.[67,68] Highly swollen cubic phases have applications in other biotechnology areas, as well as biological and physical relevance. In biosensor applications, small water channels can hamper enzymatic activity of functional enzymes encapsulated into lipid cubic mesophases.[69,70] In high resolution structure determinations *via* protein crystallization *in meso* (*i.e.*, in lipidic cubic phases),[15,28] narrow water channels can prevent the reconstitution of membrane proteins with large extracellular or intracellular domains.[13] In biology, cubic phases can have lattice dimensions on the length scales of 3000 Å,[71,72] yet lipidic cubic phases reported in the literature have lattice dimensions that are on average an order of magnitude smaller. Unraveling the mechanism behind swelling of lipid cubic phases is an active area of research.

Conclusion

Detailed mapping of phase diagrams of GMO-based systems is essential to the rational design of materials for the delivery of cargo to cells as well as protein crystallization. In this paper, we show that cubic phase formation in GMO/DOTAP is not hampered by the incorporation of a bulky PEGylated lipid (DOPE-PEG). The GMO/DOTAP/DOPE-PEG ternary mixture displays a very rich phase behavior in excess water where bicontinuous cubic phases of different symmetry are stable over a wide composition range. DOPE-PEG concentration in GMO/DOTAP/DOPE-PEG systems tunes the size of the water channels of bicontinuous cubic phases, reaching values close to 300 Å. We show that at high GMO content, DOPE-PEG plays a crucial role in determining the symmetry group of the bicontinuous phase with the primitive being preferred between 1–3 mol% and the diamond structure arising at 5 mol%. The primitive lattice is very robust and able to swell considerably more than the diamond bicontinuous cubic phase as a function of added cationic lipid.

Materials and methods

Sample preparation

1-Monooleoyl-glycerol (monoolein or GMO) was purchased from Nu-Check Prep Inc. (Elysian, MN), 1,2-dioleoyl-3-trimethyl-ammonium-propane (DOTAP) and 1,2-dioleoyl-*sn*-*glycero*-3-phosphoethanolamine-*N*-{methyoxy(polyethylene glycol)-2000} (DOPE-mPEG)

were obtained from Avanti Polar Lipids Inc. (Alabaster, AL.), and used without further purification. Lipids were dissolved in chloroform and mixed in appropriate amounts, dried with nitrogen gas while being manually rotated, and dried further under vacuum for overnight or longer. The resulting lipid films were hydrated using 60–70 °C degassed deionized water (18.2 MO cm, Milli-Q filtration system (Millipore, Germany)), and followed by at least five cycles of freeze-thaw-vortex between —196 and *ca.* 60 °C. The total lipid concentration was 250 mM for samples with 1 and 2 mol% DOPE-PEG, and 125 mM for samples with 3 and 5 mol% DOPE-PEG.

Small-angle X-ray scattering (SAXS)

Samples were transferred into quartz capillaries (Hilgenberg Glas, Germany), flame sealed with a propane/oxygen torch, protected with a bead of 5 min epoxy, and stored at 4 °C in the dark. Prior to data collection, the samples were returned to room temperature for at least 5 hours to ensure temperature equilibration. SAXS experiments were conducted in a locally built instrument (built with help from Forvis Technologies, Santa Barbara, CA) housed at the Frederick Seitz Materials Research Laboratory (Urbana-Champaign, IL) (FSMRL) or at beamline 12-ID-C of the Advanced Photon Source synchrotron at Argonne National Laboratory (Chicago, IL). The equipment at FSMRL is composed of a Xenocs GeniX3D Cu Kα ultralow divergence X-ray source (1.54 Å, 8 keV), with a divergence of 1.3 mrad and a Pilatus 300k 20 Hz hybrid pixel detector (Dectris AG, Switzerland) and a Peltier temperature controller set to 22°C. The 2D diffraction data were radially averaged using Fit2D software from ESRF. The synchrotron X-ray data was collected with 12 keV radiation, and a Pilatus detector. Distance calibration is done in both cases with silver behenate.

For bicontinuous cubic phases, water channel radius can be determined from geometric constraints.[32] Briefly, the water volume fraction (ϕ_w) is

$$\phi_w = \frac{C_w/\rho_w}{C_w/\rho_w + C_1/\rho_1} \quad (1)$$

where C_w is water weight fraction, C_l is lipid weight fraction ($C_l = 1 - C_w$), p_w is the density of water (0.9975 g mL^{-1}), p_l is the density of lipid ($p_{GMo} = 0.942$ g mL^{-1}). Knowing the lipid volume fraction ($\phi_l = 1 - \phi_w$), the lipid chain length (l) can be determined from

$$\phi_1 = 2A_0\left(\frac{l}{a}\right) + \frac{4}{3}\pi\chi\left(\frac{l}{a}\right)^3 \quad (2)$$

where a is the lattice parameter of the corresponding phase, A_0 is the ratio of the area of the minimal surface in a unit cell to (unit cell volume)$^{2/3}$, and x is the Euler-Poincare characteristic.[73] For the diamond cubic phase, $A_0 = 1.910$ and $\chi = -2$, and for the primitive cubic phase, $A_0 = 2.345$ and $\chi = -4$. The aqueous channel radius can be estimated from the following:[74]

$$r_{\mathrm{w}} = \left(-\frac{A_0}{2\pi\chi}\right)^{1/2} a - l\,. \tag{3}$$

Cryogenic transmission electron microscopy (Cryo-EM)

After the bulk of the sample have been transferred out for SAXS, 20 μL deionized water is added to the remaining residue lipids (diluted to an estimated 20 mM), and sonicated for 6 min (cycles of 5 s on, 5 s off, total time 12 min) in a cup horn sonicator (Qsonica L.L.C., Newton, CT) at 25% power for Cryo-EM. One sample (91 : 6: 3 GMO/DOTAP/DOPE-PEG) was subjected to five additional freeze-thaw-vortex cycles instead of sonication.3μL was applied onto a glow discharged (Fishione plasma cleaner, 25–40 s) 200 mesh lacey carbon-coated copper grid (Electron Microscopy Sciences, Hatfield, PA) at 90–100% humidity at 22 °C or 4 °C. Grids were blotted for 1–2 s and plunge frozen in liquid ethane using Vitrobot Mark II (FEI, Hillsboro, OR), and kept in liquid nitrogen until imaged. For imaging, the grids were transferred into a single tilt cryo holder (Gatan) for imaging on a 200 kV transmission electron microscope (JEOL 2100 cryoTEM) housed at the Frederick Seitz Materials Research Laboratory (Urbana-Champaign, IL).

Supplementary Material

Refer to Web version on PubMed Central for supplementary material.

Acknowledgements

This work was supported by the National Institutes of Health under grant no. 1DP2EB024377–01. This research used resources of the Advanced Photon Source, a U.S. Department of Energy (DOE) Office of Science User Facility operated for the DOE Office of Science by Argonne National Laboratory under Contract No. DE-AC02–06CH11357 and was carried out in part in the Frederick Seitz Materials Research Laboratory Research Facilities, University of Illinois. We thank Dr. Soenke Seifert of beamline 12-ID-C at APS for his assistance and hospitality, and Dylan Steer for technical assistance.

References

1. Almsherqi ZA, Landh T, Kohlwein SD and Deng Y, Int. Rev. Cell Mol. Biol, 2009, 274, 275–342. [PubMed: 19349040]
2. Xiao Q, Wang Z, Williams D, Leowanawat P, Peterca M, Sherman SE, Zhang S, Hammer DA, Heiney PA, King SR, Markovitz DM, Andre S, Gabius HJ, Klein ML and Percec V, ACS Cent. Sci, 2016, 2, 943–953. [PubMed: 28058284]
3. Shah JC, Sadhale Y. and Chilukuri DM, Adv. Drug Delivery Rev, 2001, 47, 229–250.
4. Mulet X, Boyd BJ and Drummond CJ, J. Colloid Interface Sci, 2013, 393, 1–20. [PubMed: 23237762]
5. Leal C, Bouxsein NF, Ewert KK and Safinya CR, J. Am. Chem. Soc, 2010, 132, 16841–16847. [PubMed: 21028803]
6. Kim H. and Leal C, ACS Nano, 2015, 9, 10214–10226. [PubMed: 26390340]
7. Kang M. and Leal C, Adv. Funct. Mater, 2016, 26, 5610–5620.
8. Kim H, Sung J, Chang Y, Alfeche A. and Leal C, ACS Nano, 2018, 12, 9196–9205. [PubMed: 30081623]
9. Vallooran JJ, Handschin S, Pillai SM, Vetter BN, Rusch S, Beck HP and Mezzenga R, Adv. Funct. Mater, 2016, 26, 181–190.

10. Nazaruk E, Bilewicz R, Lindblom G. and Lindholm-Sethson B, Anal. Bioanal. Chem, 2008, 391, 1569–1578. [PubMed: 18488208]
11. Gupta A, Stait-Gardner T, De Campo L, Waddington LJ, Kirby N, Price WS and Moghaddam MJ, J. Mater. Chem. B,2014, 2, 1225–1233.
12. Bazylinska U, Kulbacka J, Schmidt J, Talmon Y. and Murgia S, J. Colloid Interface Sci, 2018, 522, 163–173. [PubMed: 29601958]
13. Zabara A, Chong JTY, Martiel I, Stark L, Cromer BA, Speziale C, Drummond CJ and Mezzenga R, Nat. Commun, 2018, 9, 544–552. [PubMed: 29416037]
14. Cherezov V, Clogston J, Misquitta Y, Abdel-Gawad W. and Caffrey M, Biophys. J, 2002, 83, 3393–3407. [PubMed: 12496106]
15. Cherezov V, Curr. Opin. Struct. Biol, 2011, 21, 559–566. [PubMed: 21775127]
16. Caffrey M, Acta Crystallogr., Sect. F: Struct. Biol. Commun, 2015, 71, 3–18. [PubMed: 25615961]
17. Mezzenga R, Schurtenberger P, Burbidge A. and Michel M, Nat. Mater, 2005, 4, 729–740. [PubMed: 16195765]
18. Larsson K, J. Phys. Chem, 1989, 93, 7304–7314.
19. Luzzati V, Gulik-Krzywicki T. and Tardieu A, Nature, 1968, 218, 1031–1034. [PubMed: 5656617]
20. Ellison LJ, Michel DJ, Barmes F. and Cleaver DJ, Phys. Rev. Lett, 2006, 97, 237801.
21. Israelachvili JN, Marcelja S. and Horn RG, Q. Rev. Biophys, 1980, 13, 121–200. [PubMed: 7015403]
22. Shearman GC, Ces O. and Templer RH, Soft Matter, 2010, 6, 256–262.
23. Bruinsma R, Phys J.. II, 1992, 2, 425–451.
24. Barriga HMG, Tyler AII, McCarthy NLC, Parsons ES, Ces O, Law RV, Seddon JMand Brooks NJ, Soft Matter, 2015, 11, 600–607. [PubMed: 25430049]
25. Kim H, Song Z. and Leal C, Proc. Natl. Acad. Sci. U. S. A,2017,201710774.
26. Tyler AII, Barriga HMG, Parsons ES, McCarthy NLC, Ces O, Law RV, Seddon JM and Brooks NJ, Soft Matter, 2015, 11, 3279–3286. [PubMed: 25790335]
27. Angelov B, Angelova A, Ollivon M, Bourgaux C. and Campitelli A, J. Am. Chem. Soc, 2003, 125, 7188–7189. [PubMed: 12797787]
28. Cherezov V, Clogston J, Papiz MZ and Caffrey M, J. Mol. Biol, 2006, 357, 1605–1618. [PubMed: 16490208]
29. Engblom J, Miezis Y, Nylander T, Razumas V. and Larsson K, Surface and Colloid Science, Springer Berlin Heidelberg, Berlin, Heidelberg, 2000, vol. 116, pp. 9–15.
30. Larsson K, Nature, 1983, 304, 664.
31. Andersson S, Hyde ST, Larsson K. and Lidin S, Chem. Rev, 1988, 88, 221–242.
32. Turner DC, Wang Z-G, Gruner SM, Mannock DA and McElhaney RN, J. Phys. II, 1992, 2, 2039–2063.
33. Kraineva J, Smirnovas V. and Winter R, Langmuir, 2007, 23, 7118–7126. [PubMed: 17523690]
34. Maskery I, Sturm L, Aremu AO, Panesar A, Williams CB, Tuck CJ, Wildman RD, Ashcroft IA and Hague RJM, Polymer, 2018, 152, 62–71.
35. Freag MS, Elnaggar YSR, Abdelmonsif DA and Abdallah OY, Int. J. Nanomed, 2016, 11, 4799–4818.
36. Kang M, Kim H. and Leal C, Curr. Opin. Colloid Interface Sci, 2016, 26, 58–65. [PubMed: 28496379]
37. Leal C, Ewert KK, Bouxsein NF, Shirazi RS, Li Y. and Safinya CR, Soft Matter, 2013, 9, 795–804. [PubMed: 23476712]
38. International tables for crystallography volume A: space-group symmetry, ed. Aroyo MI, International Union of Crystallography, Chester, England, 6th edn, 2016.
39. Almgren M, Edwards K. and Karlsson G, Colloids Surf., A, 2000, 174, 3–21.
40. Helvig S, Azmi IDM, Moghimi SM and Yaghmur A, AIMS Biophys, 2015, 2, 116–130.
41. Sagalowicz L, Michel M, Adrian M, Frossard P, Rouvet M, Watzke HJ, Yaghmur A, De Campo L, Glatter O. and Leser ME, J. Microsc, 2006, 221, 110–121. [PubMed: 16499550]
42. Kuntsche J, Horst JC and Bunjes H, Int. J. Pharm, 2011, 417, 120–137. [PubMed: 21310225]

43. Mezzenga R, Meyer C, Servais C, Romoscanu AI, Sagalowicz L. and Hayward RC, Langmuir, 2005, 21, 3322–3333. [PubMed: 15807570]
44. Pitzalis P, Monduzzi M, Krog N, Larsson H, Ljusberg-Wahren H. and Nylander T, Langmuir, 2000, 16, 6358–6365.
45. Abdelwahed W, Degobert G, Stainmesse S. and Fessi H, Adv. Drug Delivery Rev, 2006, 58, 1688–1713.
46. Li F, Wang T, He HB and Tang X, Int. J. Pharm, 2008, 349, 291–299. [PubMed: 17889466]
47. Morais ARDV, Alencar ÉDN, Xavier Junior FH, De Oliveira CM, Marcelino HR, Barratt G, Fessi H, Do Egito EST and Elaissari A, Int. J. Pharm, 2016, 503, 102–114. [PubMed: 26943974]
48. Zhang H, Ice Templating and Freeze-drying for Porous Materials and their Applications, Wiley-VCH, Weinheim, 2018.
49. Karami Z. and Hamidi M, Drug Discovery Today, 2016, 21, 789–801. [PubMed: 26780385]
50. Koynova R, Tenchov B. and Macdonald RC, ACS Biomater. Sci. Eng, 2015, 1, 130–138.
51. Kraineva J, Narayanan RA, Kondrashkina E, Thiyagarajan P. and Winter R, Langmuir, 2005, 21, 3559–3571. [PubMed: 15807602]
52. Mulet X, Kennedy DF, Conn CE, Hawley A. and Drummond CJ, Int. J. Pharm, 2010, 395, 290–297. [PubMed: 20580796]
53. Meikle TG, Zabara A, Waddington LJ, Separovic F, Drummond CJ and Conn CE, Colloids Surf., B, 2017,152, 143–151.
54. Aota-Nakano Y, Li SJ and Yamazaki M, Biochim. Biophys. Acta, 1999, 1461, 96–102. [PubMed: 10556491]
55. Clogston J, Craciun G, Hart DJ and Caffrey M, J. Controlled Release, 2005, 102, 441–461.
56. Leal C, Rögnvaldsson S, Fossheim S, Nilssen EA and Topgaard D, J. Colloid Interface Sci, 2008, 325, 485–493. [PubMed: 18589432]
57. Gustafsson J, Ljusberg-Wahren H, Almgren M. and Larsson K, Langmuir, 1996, 12, 4611–4613.
58. Nakano M, Kamo T, Sugita A. and Handa T, J. Phys. Chem. B, 2005, 109, 4754–4760. [PubMed: 16851558]
59. Angelov B, Angelova A, Drechsler M, Garamus VM, Mutafchieva R. and Lesieur S, Soft Matter, 2015, 11, 3686–3692. [PubMed: 25820228]
60. Angelov B, Angelova A, Filippov SK, Narayanan T, Drechsler M, Stepanek P, Couvreur P. and Lesieur S, J. Phys. Chem. Lett, 2013, 4, 1959–1964. [PubMed: 26283134]
61. Angelova A, Drechsler M, Garamus VM and Angelov B, ACS Omega, 2018, 3, 3235–3247. [PubMed: 30023865]
62. Valldeperas M, Wisniewska M, Ram-On M, Kesselman E, Danino D, Nylander T. and Barauskas J, Langmuir, 2016, 32, 8650–8659. [PubMed: 27482838]
63. Siekmann B, Bunjes H, Koch MHJ and Westesen K, Int. J. Pharm, 2002, 244, 33–43. [PubMed: 12204563]
64. Awad TS, Okamoto Y, Masum SM and Yamazaki M, Langmuir, 2005, 21, 11556–11561. [PubMed: 16316079]
65. Nazaruk E, Gorecka E, Osornio YM, Landau EM and Bilewicz R, J. Electroanal. Chem, 2018, 819, 269–274.
66. Yaghmur A, Laggner P, Zhang S. and Rappolt M, PLoS One, 2007, 2, e479–e488. [PubMed: 17534429]
67. Negrini R. and Mezzenga R, Langmuir, 2012, 28, 16455–16462. [PubMed: 23116138]
68. Zabara A. and Mezzenga R, J. Controlled Release, 2014, 188, 31–43.
69. Sun W, Vallooran JJ, Zabara A. and Mezzenga R, Nanoscale, 2014, 6, 6853–6859. [PubMed: 24831024]
70. Zabara A. and Mezzenga R, Soft Matter, 2012, 8, 6535.
71. Almsherqi ZA, Kohlwein SD and Deng Y, J. Cell Biol, 2006, 173, 839–844. [PubMed: 16785319]
72. Deng Y, Marko M, Buttle KF, Leith A, Mieczkowski M. and Mannella CA, J. Struct. Biol, 1999, 127, 231–239. [PubMed: 10544048]
73. Qiu H. and Caffrey M, J. Phys. Chem. B, 1998, 102, 4819–4829.

74. Anderson DM, Gruner SM and Leibler S, Proc. Natl. Acad. Sci. U. S. A, 1988, 85, 5364–5368. [PubMed: 3399497]

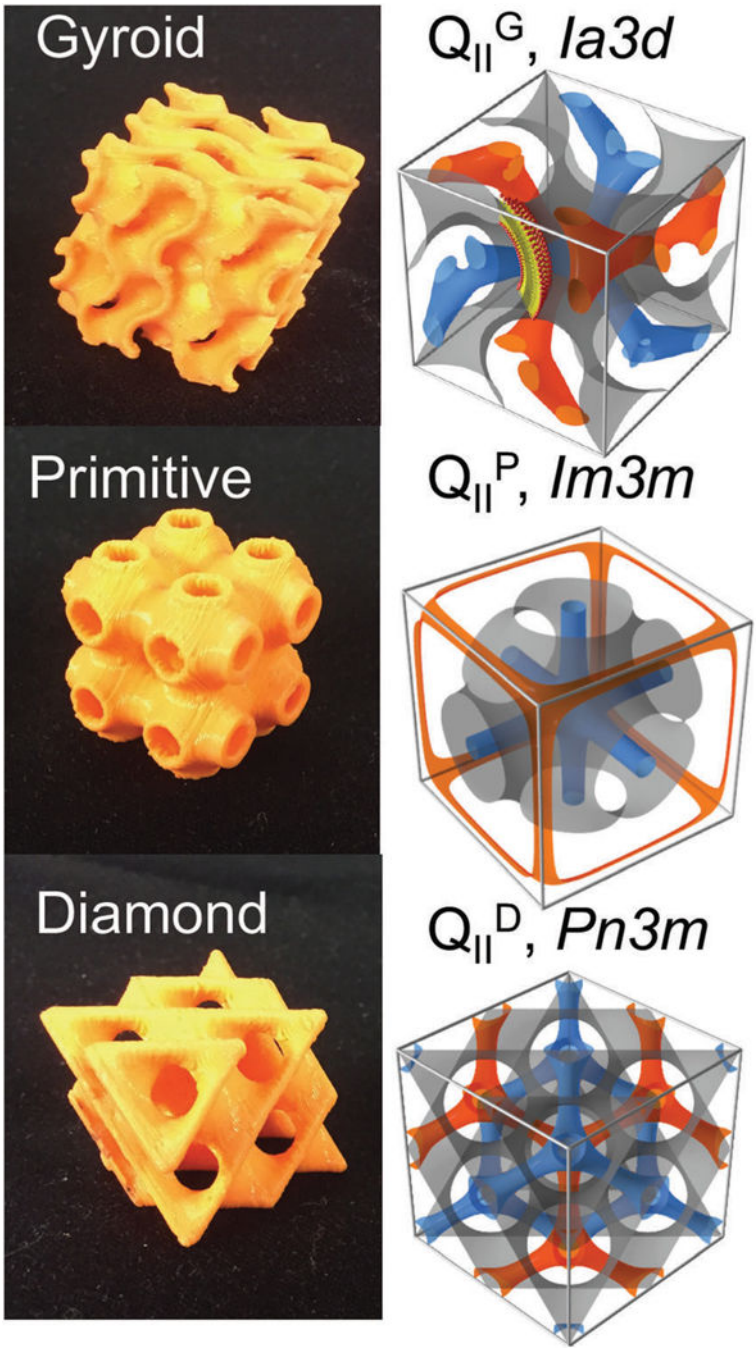

Fig. 1.

Bicontinuous cubic structures and their unit cells. Two independent water channels (blue and orange) are separated by a lipid bilayer (bilayer mid-planes represented by the orange structures in the left images and gray on the right).

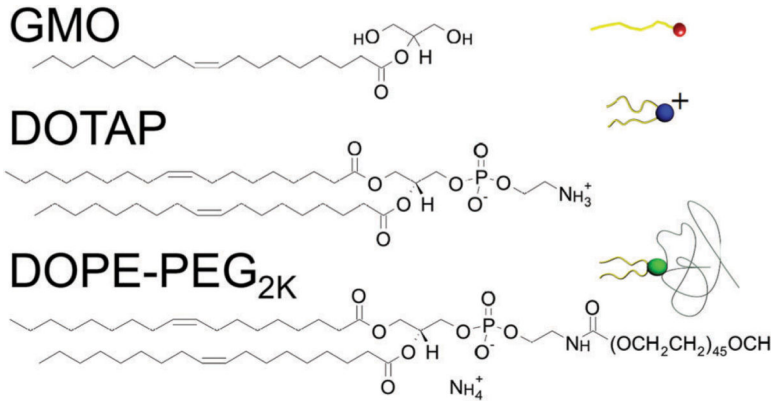

Fig. 2.

Molecular structures of cationic lipid (DOTAP), cubic-phase forming lipid (GMO), and anionic PEGylated lipid (DOPE-PEG).

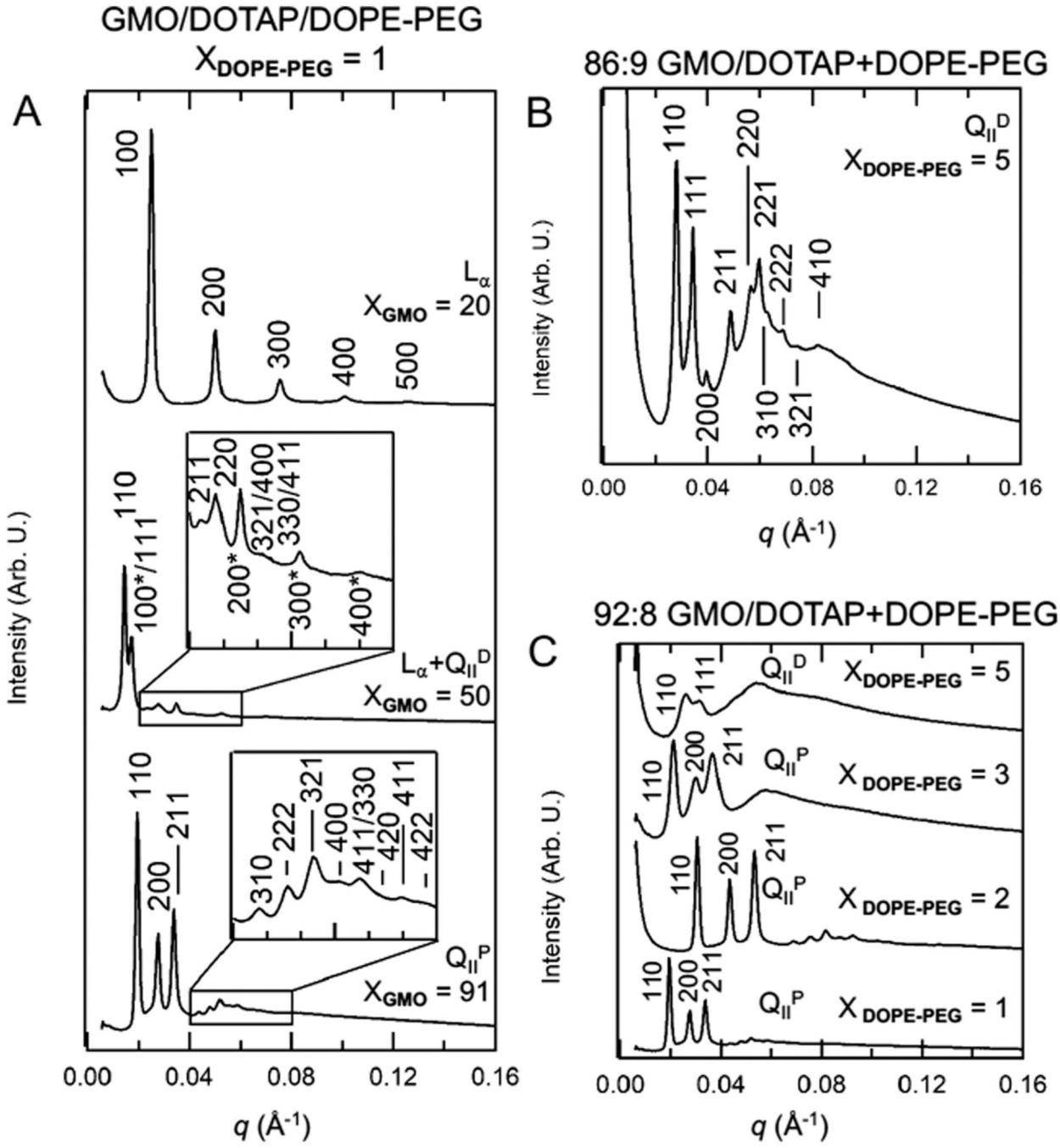

Fig. 3.

Representative radially integrated SAXS diffraction patterns of GMO/DOTAP/DOPE-PEG. (A) DOPE-PEG concentration is fixed at 1 mol%, and GMO/DOTAP ratio is varied. Miller indices are shown for Bragg reflections for lamellar (L_α) phase (20 mol% GMO), diamond $\left(Q_{\|}^{D}\right)$+L_α coexistence (50 mol% GMO), and primitive cubic $\left(Q_{\|}^{P}\right)$ phase (91 mol% GMO). When in coexistence, lamellar indices are marked with asterisks (*). (B) Representative X-ray diffractogram for the diamond cubic phase $\left(Q_{\|}^{D}\right)$ obtained at DOPE-PEG 5 mol%. (C) At

high GMO/DOTAP ratios (*e.g.,* 92 : 8 GMO/DOTAP), the primitive cubic phase $\left(Q_{\|}^{P}\right)$ dominates at 1–3 mol% DOPE-PEG and the diamond cubic phase $\left(Q_{\|}^{D}\right)$ dominates at 5 mol % DOPE-PEG.

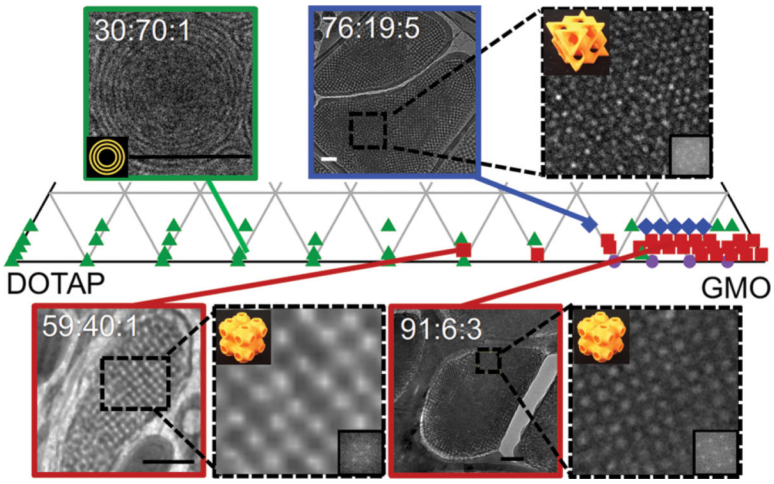

Fig. 4.

Partial phase diagram of GMO/DOTAP/DOPE-PEG in excess water constructed from SAXS data. Multilamellar vesicles (MLV) were observed at low GMO concentration (≤*ca*. 40 : 60 GMO/DOTAP), and bicontinuous cubic phases were observed at high GMO content (≥*ca*. 85:15 GMO/DOTAP). Symbols identify structures observed with SAXS: lamellar (green triangle), primitive bicontinuous cubic (red square), diamond bicontinuous cubic (blue diamond), gyroid bicontinuous cubic (purple circle). In some instances, a reentrant lamellar phase is observed at high GMO content. Cryo-EM micrographs are consistent with SAXS data. With 5 mol% DOPE-PEG, diamond bicontinuous cubic phases are observed (*e.g.*, 76 : 19 : 5) and the primitive lattices are preferred for 1 mol% (59 : 40 : 1) and 3 mol% (91 : 6 : 3). Fast Fourier transforms of the enlarged areas (inset) confirm the space group symmetries of the cubic phases (orange 3D models). Scale bars are 200 nm.

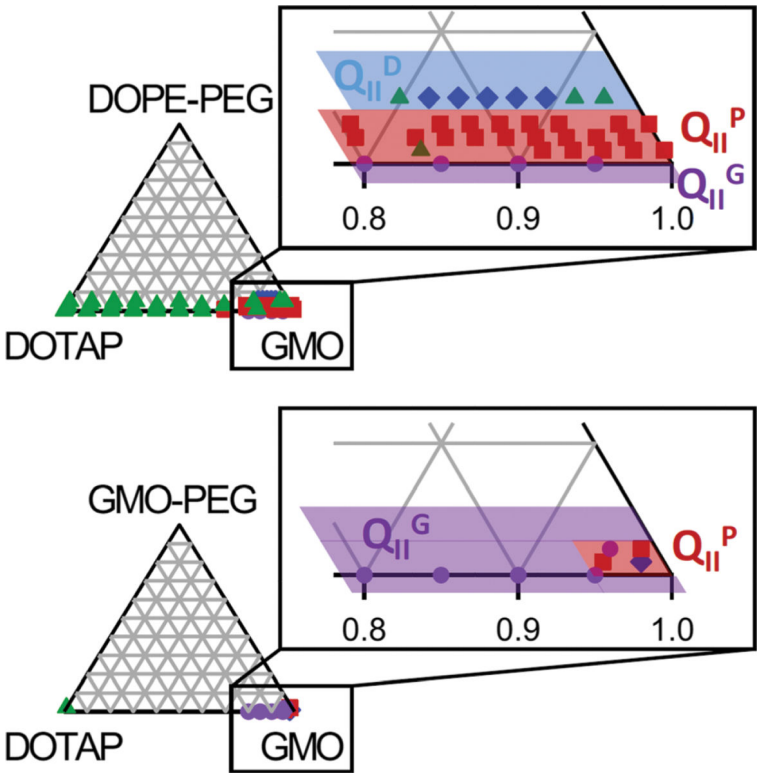

Fig. 5.

Comparison of partial phase diagrams of GMO/DOTAP/DOPE-PEG and GMO/DOTAP/GMO-PEG in excess water. Primitive cubic phases $\left(Q_{\|}^{P}\right)$ occupy a larger composition range in DOPE-PEG ternary mixtures than in GMO-PEG ternary mixtures, where the gyroid $\left(Q_{\|}^{G}\right)$ is the dominant structure. GMO/DOTAP and GMO/DOTAP/GMO-PEG data were extracted from Leal *et al.*[5] and Kim *et al.*,[6] respectively.

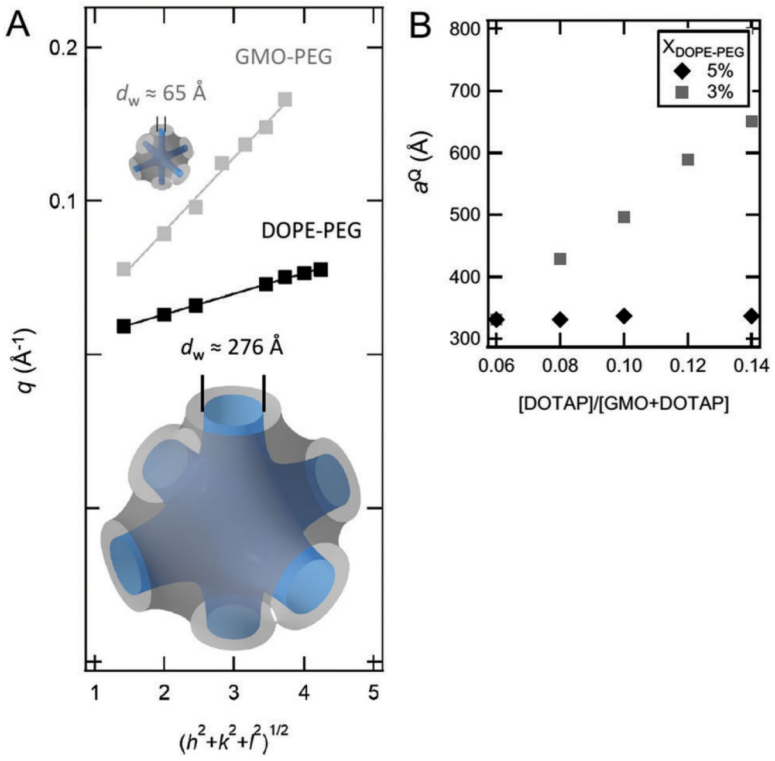

Fig. 6.

Large cubic phase water channels. Cubic phases made with DOPE-PEG can swell more than those made with GMO-PEG. (A) Comparison of the primitive cubic phases of 95 : 4 : 1 GMO/DOTAP/DOPE-PEG (black) and 95 : 4 : 1 GMO/DOTAP/GMO-PEG (gray). Wave-vector q *versus* $(h^2 + k^2 + l^2)^{1/2}$ shows the expected straight line with slope $2\pi/a^Q$, where a^Q is the lattice spacing. The lattice spacing of 160 Å for the GMO-PEG mixture corresponds to estimated water channel diameter (d_W) of 65 Å, and the lattice spacing of 484 A for DOPE-PEG mixture corresponds to d_W = 276 Å. (B) Comparison of lattice spacing (a^Q) for GMO/DOTAP/DOPE-PEG primitive (square symbols) *vs.* diamond (diamond symbols) cubic structures.